

Polar amplification of Pliocene climate by elevated trace gas radiative forcing

Hopcroft, Peter; Ramstein, Gilles; Pugh, Thomas; Hunter, Stephen; Murguia-Flores, Fabiola; Quiquet, Aurelien; Sun, Yong; Tan, Ning; Valdes, Paul J.

DOI:
[10.1073/pnas.2002320117](https://doi.org/10.1073/pnas.2002320117)

License:
None: All rights reserved

Document Version
Peer reviewed version

Citation for published version (Harvard):
Hopcroft, P, Ramstein, G, Pugh, T, Hunter, S, Murguia-Flores, F, Quiquet, A, Sun, Y, Tan, N & Valdes, PJ 2020, 'Polar amplification of Pliocene climate by elevated trace gas radiative forcing', *National Academy of Sciences. Proceedings*, vol. 117, no. 38, pp. 23401-23407. <https://doi.org/10.1073/pnas.2002320117>

[Link to publication on Research at Birmingham portal](#)

General rights

Unless a licence is specified above, all rights (including copyright and moral rights) in this document are retained by the authors and/or the copyright holders. The express permission of the copyright holder must be obtained for any use of this material other than for purposes permitted by law.

- Users may freely distribute the URL that is used to identify this publication.
- Users may download and/or print one copy of the publication from the University of Birmingham research portal for the purpose of private study or non-commercial research.
- User may use extracts from the document in line with the concept of 'fair dealing' under the Copyright, Designs and Patents Act 1988 (?)
- Users may not further distribute the material nor use it for the purposes of commercial gain.

Where a licence is displayed above, please note the terms and conditions of the licence govern your use of this document.

When citing, please reference the published version.

Take down policy

While the University of Birmingham exercises care and attention in making items available there are rare occasions when an item has been uploaded in error or has been deemed to be commercially or otherwise sensitive.

If you believe that this is the case for this document, please contact UBIRA@lists.bham.ac.uk providing details and we will remove access to the work immediately and investigate.

Polar amplification of Pliocene climate by elevated trace gas radiative forcing

Peter O. Hopcroft^{a,1}, Gilles Ramstein^b, Thomas A.M. Pugh^{a,c}, Stephen J. Hunter^d, Fabiola Murguía-Flores^e, Aurélien Quiquet^{b,f}, Yong Sun^{b,g}, Ning Tan^{b,h}, and Paul J. Valdes^e

^aSchool of Geography, Earth & Environmental Sciences, University of Birmingham, U.K. B15 2TT; ^bLaboratoire des Sciences du Climat et de l'Environnement, LSCE/IPSL, CEA-CNRS-UVSQ, Université Paris-Saclay, F-91191 Gif-sur-Yvette, France.; ^cBirmingham Institute of Forest Research, University of Birmingham, U.K. B15 2TT; ^dSchool of Earth and Environment, University of Leeds, Leeds, UK.; ^eBristol Research Initiative for the Dynamic Global Environment, School of Geographical Sciences, University of Bristol, U.K. BS8 1SS.; ^fInstitut Louis Bachelier, Chair Energy and Prosperity, Paris, 75002, France.; ^gState Key Laboratory of Numerical Modelling for Atmospheric Sciences and Geophysical Fluid Dynamics, Institute of Atmospheric Physics, Chinese Academy of Sciences, Beijing, China.; ^hKey Laboratory of Cenozoic Geology and Environment, Institute of Geology and Geophysics, Chinese Academy of Sciences, Beijing 100029, China.

This manuscript was compiled on July 16, 2020

1 **Warm periods in Earth's history offer opportunities to understand**
2 **the dynamics of the Earth System under conditions that are simi-**
3 **lar to those expected in the near future. The mid-Pliocene warm pe-**
4 **riod (mPWP) from 3.3-3.0 million years ago, is the most recent time**
5 **when atmospheric CO₂ levels were as high as today. However, cli-**
6 **mate model simulations of the Pliocene underestimate high latitude**
7 **warming that has been reconstructed from fossil pollen samples and**
8 **other geological archives. One possible reason for this is that en-**
9 **hanced non-CO₂ trace gas radiative forcing during the Pliocene, in-**
10 **cluding from methane (CH₄), has not been included in modelling. We**
11 **use a suite of terrestrial biogeochemistry models forced with mPWP**
12 **climate model simulations from four different climate models, to pro-**
13 **duce the first comprehensive reconstruction of the mPWP CH₄ cy-**
14 **cle, including uncertainty. We simulate an atmospheric CH₄ mixing**
15 **ratio of 1000-1200 ppbv, which in combination with estimates of radi-**
16 **ative forcing from N₂O and O₃, contributes a non-CO₂ radiative for-**
17 **cing of 0.9 Wm⁻² (range 0.6-1.1), which is 43% (range 36-56%) of the**
18 **CO₂ radiative forcing used in mPWP climate simulations. This addi-**
19 **tional forcing would cause a global surface temperature increase of**
20 **0.6-1.0 °C, with amplified changes at high-latitudes, improving agree-**
21 **ment with geological evidence of mid-Pliocene climate. We conclude**
22 **that natural trace gas feedbacks are critical for interpreting climate**
23 **warmth during the Pliocene and potentially many other warm phases**
24 **of the Cenozoic. These results also imply that using Pliocene CO₂**
25 **and temperature reconstructions alone, may lead to overestimates**
26 **of the "fast" or "Charney" climate sensitivity.**

Methane | Pliocene | GCM | Trace gas | Biogeochemistry | Wetland

1. Introduction

2 The mid-Pliocene warm period around 3.3-3.0 million years ago
3 was the last period in Earth's history when atmospheric CO₂
4 was comparable to today's level, at approximately 400 ppmv
5 (1-4). The mPWP could therefore provide useful information
6 on the response of the Earth System to greenhouse gas-induced
7 warming, that is relevant to the future evolution of the Earth
8 System under continued anthropogenic greenhouse gas emis-
9 sions (5-9). According to syntheses of reconstructed surface
10 temperatures from geological archives on land (10) and in
11 the ocean (11, 12), the Earth was globally warmer than the
12 pre-industrial, with a significant polar amplification especially
13 in the Northern Hemisphere. The warmer conditions acted to
14 reduce global ice volume, so that sea-level was around 20 m
15 higher than present (13-15).

16 The Pliocene Model Intercomparison Project (PlioMIP) is
17 a co-ordinated study of climate model responses to Pliocene

boundary conditions (16, 17) aimed at quantifying the un-
derlying drivers of warmth during this time and to better
understand the Earth System response to an atmospheric CO₂
concentration of ~400 ppmv. The results from the first phase
(PlioMIP1) showed that coupled general circulation models
(GCMs) failed to reproduce high-latitude warming seen in
reconstructions (16). Several hypotheses could explain why
the model simulations underestimate warming, including the
role of orbitally induced climate variability (16), the configura-
tion of ocean gateways and palaeogeography (e.g. 18, 19) and
radiative forcing from trace gases other than CO₂ (20). Whilst
several studies have addressed the first three possibilities, the
contribution of the atmospheric methane, nitrous oxide and
ozone (CH₄, N₂O, O₃) have not been considered together.

At present CH₄ is the second most important anthropogenic
greenhouse gas after CO₂ (21). Its nearly three-fold concentra-
tion increase since CE 1750 is responsible for approximately
25% of the greenhouse gas radiative forcing. We know that
variations in CH₄ are huge in intensity and abrupt during
the Anthropocene relative to the past several thousand years.
Before widespread direct atmospheric monitoring, CH₄ could
only be traced through air bubbles trapped in polar ice-cores.

Significance Statement

Warm periods in Earth's history provide the only empirical evidence of how the climate system responds to raised atmospheric carbon dioxide (CO₂) levels. The mid-Pliocene, 3.3-3.0 million years ago, was the last time when CO₂ levels were as high as today. However, climate model simulations of the Pliocene underestimate the warming that has been reconstructed from geological archives. Using a numerical model of the global methane cycle we show that the inclusion of enhanced concentrations of non-CO₂ trace gases, could have been responsible for an additional warming of 0.6-1.0°C, with larger increases over northern landmasses. These findings demonstrate the importance of trace gas climate forcing both for the Pliocene and potentially warm periods during much of Earth's recent history.

POH, GR, and PJV conceived research. POH developed offline models for wetlands, soil NO_x, termites. TP and POH carried out LPJ-GUESS simulations, NT, CC, SJH ran GCM simulations. FM ran soil CH₄ uptake model simulations. All authors contributed to interpreting the results and writing the manuscript.

The authors declare no conflict of interest.

¹To whom correspondence should be addressed. E-mail: p.hopcroft@bham.ac.uk

40 These ice-core records provide robust evidence that CH₄ is
41 very sensitive to climate, with higher values during warmer pe-
42 riods, and with large-amplitude rapid variations during abrupt
43 climate events (22, 23). Nitrous oxide (N₂O) also displays sim-
44 ilar characteristics (24), whilst O₃ and many other important
45 atmospheric constituents (e.g. OH) cannot be reconstructed
46 from ice-core gas samples. Before 800,000 years ago, variations
47 in all trace gases with the exception of CO₂, are essentially
48 unknown, and must therefore be simulated using models (e.g.
49 25).

50 Beerling et al. (2009) simulated enhanced wetland emissions
51 during the Pliocene but did not link this with other methane
52 sources or sinks(26). Unger & Yue, 2014(20) (UY14 hereafter)
53 simulated an increase in CH₄ lifetime by 23-31% during the
54 Pliocene (for CH₄=1000 - 2000 ppbv) and an increase in tropo-
55 spheric O₃ by 21-25% which contributed a radiative forcing of
56 approximately 0.3 Wm⁻². However, this CH₄ lifetime increase
57 is partly caused by the self-feedback (e.g. 27), a function of
58 the prescribed CH₄ concentration in the model. Other than a
59 model study of the Eocene and late Cretaceous super-warm
60 periods (28), there is no comprehensive understanding of how
61 trace gases may have affected pre-Quaternary warm periods
62 like the Pliocene.

63 We address this with an ensemble of terrestrial biogeochem-
64 istry simulations for the Pliocene. In combination with climate
65 fields from several GCM simulations of the Pliocene we develop
66 the first estimate of the Pliocene global CH₄ source, CH₄ sinks
67 and thereby the CH₄ concentration, and CH₄ radiative forcing,
68 including uncertainty. We combine these with estimates of
69 N₂O and O₃ radiative forcing to evaluate for the first time
70 how all of these trace gases may have determined the climate
71 during the Pliocene.

72 2. Results

73 **A. Emissions of CH₄ and Other Trace Gases.** Our approach
74 follows that used for modelling of the Quaternary CH₄ varia-
75 tions (25, 29, 30). We drive the LPJ-GUESS dynamic global
76 vegetation model (31, 32) with climate simulations from four
77 models used in the Pliocene Model Intercomparison Project
78 phases 1 and 2 and simulate the key trace gas emissions at
79 the land surface, including CH₄, emissions from wildfires, non-
80 methane biogenic volatile organic compounds (NBVOCs) from
81 vegetation and soil nitrogen oxides (NO_x), see SI Appendix,
82 Fig. S1. Assuming that the Pliocene is a quasi-equilibrium
83 climate state, we do not account for any increased emissions
84 from marine clathrates or permafrost which are likely more
85 sensitive to abrupt warming (33). We use PlioMIP phase
86 1 (experiment 2) simulations (34) with CCSM4, GISS-E2-
87 R and IPSL-CM5A-LR and PlioMIP phase 2 (Eoi⁴⁰⁰) (16)
88 simulations with IPSL-CM5A-LR and HadCM3-M21. In all
89 Pliocene climate model simulations the orography, land-ice
90 and vegetation are based on geological reconstructions for the
91 Pliocene (35, 36) and the mixing ratio of atmospheric CO₂
92 is increased from 280 ppbv in the pre-industrial to 400 or
93 405 ppbv. We also incorporate HadCM3 PlioMIP phase 2
94 simulations performed with atmospheric CO₂ mixing ratios of
95 450 (50) and 490 ppmv which are labelled Eoi⁴⁵⁰ and Eoi⁴⁹⁰,
96 respectively. All climate simulations are described in Materials
97 and Methods.

98 We estimate the CH₄ lifetime and the resultant concentra-
99 tion of CH₄ using a simplified offline one-box model of the

atmospheric CH₄ chemistry (37) and radiative forcing (38).
With this we do not resolve atmospheric transport or detailed
chemical pathways, but we are able to quantify uncertainty
by sampling the model stochastically. See Methods and Sup-
porting Information SI Appendix, Table S2 for full details of
all models used.

All CH₄ emissions increase in response to the simulated
Pliocene climate conditions (see SI Appendix, Table S1). De-
spite warmer and in many places wetter conditions (see SI
Appendix, Fig. S2), wetland area increases only marginally,
but the emissions increase by 20-46%. Emissions increase no-
tably in the Sahel region of North Africa in all models, and in
South Africa in all models except GISS. Elsewhere, emissions
increase in South East Asia in all models except GISS and
Australia in all models except CCSM4 and GISS. GISS shows
the largest emissions increase of all models over the Amazon,
whereas both IPSL simulations show a slight reduction in
this region. A factor separation approach summarised in SI
Appendix, Table S3, demonstrates that increased Pliocene
temperature enhance emissions in all models. In HadCM3
and GISS wetter soils also promote emissions, but are less
important in the other GCMs. Soil carbon stocks act to re-
duce emissions in HadCM3, and increase emissions in CCSM4,
but have much less impact in the other models. Wildfire,
and termite emissions also increase by 50-83% and 21-37%,
respectively and soil uptake (at pCH₄=715 ppmv) increases by
8-27%. Isoprene emissions increase by 5-40% and monoterpene
changes by -9 to +7%. These ranges span the different climate
models used to drive each emissions scheme.

B. CH₄ Chemical Lifetime and Radiative Forcing. Although in-
creased emissions will translate into elevated atmospheric con-
centration, the concentration is also dependent on the lifetime,
which is influenced by other trace gas emissions and the phys-
ical state of the atmosphere. The change in CH₄ lifetime,
Pliocene minus pre-industrial, is summarised for each GCM
in figure 1. Increased CH₄ emissions from wetlands, wildfires
and termites contribute a positive lifetime anomaly through
the self-feedback effect. Additional NMVOC emissions (CO
and isoprene) from wildfires and vegetation enhance the life-
time slightly. The higher global temperatures and associated
humidity increase act to offset some of this lifetime increase
in each model. This is because the reaction rate of CH₄ with
OH scales with temperature and the production of OH which
oxidises CH₄, increases with water vapour availability and
hence temperature (e.g. 37, 39). BVOCs are the most model-
dependent term, with a strong increase in emissions during
the Pliocene in IPSL and HadCM3 but not in the other two
GCMs. This is most likely a result of the differences in the
response of the tropical hydrological cycle. Soil NO_x shows
agreement across the four climate models. The results are
also in agreement with the results of UY14. Lightning NO_x
increase and increased O₃ in the troposphere (both taken from
UY14) have opposing influences on the Pliocene lifetime.

As the CH₄ lifetime is dependent on the CH₄ level, there is
a non-linearity which means that the total change in lifetime
does not equal the sum of these individual terms. The net
change is positive for HadCM3 and both IPSL simulations
and very weakly negative in the other two models. This is
mostly due to the much stronger BVOC emission term in the
former two models.

The results of the sampling of the total Pliocene minus

161 pre-industrial CH₄ radiative forcing are shown in figure 2.
162 The mean±1 standard deviation anomalies are 0.16±0.02,
163 0.20±0.03, 0.21±0.03 and 0.33±0.05 Wm⁻² for CCSM4, GISS,
164 IPSL and HadCM3, respectively. The combined mean and
165 1σ range is 0.22±0.07 Wm⁻². The total uncertainty in this
166 estimate is dominated by the choice of climate simulation.

167 3. Discussion

168 **A. Total Radiative forcing.** The global mean radiative forcing
169 due to the CO₂ concentration of 400 ppm during the Pliocene
170 is around 2.0±0.3 Wm⁻². We approximate N₂O radiative
171 forcing based on natural variations in these three greenhouse
172 gases through the late Quaternary as 15% of the combined
173 CO₂ and CH₄ radiative forcing(40). Radiative forcing by O₃
174 is 0.29 Wm⁻² as simulated for CH₄=1000 ppbv by UY14(20).
175 This positive radiative forcing is partly due to a simulated
176 increase in emissions of O₃ precursors, consistent with our
177 simulated emissions (SI Appendix, Table S1). The uncertainty
178 on the O₃ radiative forcing is calculated by scaling with the
179 CH₄ concentration, which in three sensitivity simulations by
180 (20) shows an approximately logarithmic dependence. O₃
181 is also created as a by-product of CH₄ emissions, thus it is
182 partially included in the O₃ radiative forcing and in our indirect
183 CH₄ radiative forcing. Hence we reduce our total forcing using
184 the combined factor for O₃ radiative forcing from CH₄ as in SI
185 Appendix, Table S4, to avoid double counting. Together with
186 a CH₄ radiative forcing, we derive an approximate radiative
187 forcing due to other non-CO₂ well-mixed GHGs of 0.8 (0.62-
188 1.02) Wm⁻² as summarized in table 1.

189 The rate of methane radiative forcing increase per degree
190 of global mean temperature change (see also 41) is a useful
191 property to compare time periods or models. We denoted
192 this as γ_{fCH_4} and it ranges from 89-113 mWm⁻²/K across
193 the 5 climate model simulations, with the lowest value sim-
194 ulated by CCSM4 and the highest by HadCM3. This range
195 slightly exceeds the observed value of 68 (57-85) mWm⁻²/K
196 derived from the last glacial maximum to the late-Holocene
197 pre-industrial (22, 42). It is consistent with simulated values
198 of 97-119 mWm⁻²/K for the Early Eocene and 89 mWm⁻²/K
199 for the Late Cretaceous calculated with a coupled climate-
200 chemistry modelling framework (28), for which the direct
201 radiative forcing values have been augmented here following a
202 recent update (38).

203 The Pliocene climate may have induced changes in the
204 emissions and lifetime of natural aerosols. UY14 simulated
205 a net cooling by nitrate, particulate organic matter and bio-
206 genic secondary organic aerosols (SOA) and a warming effect
207 from black carbon, leading to a negative aerosol forcing of
208 -0.4 Wm⁻² (20). We simulate smaller changes in emissions
209 from biomass burning (+50-84% versus a +101% by UY14)
210 and BVOCs (precursors of SOA: +5-40% versus +50% by
211 UY14), and so this would likely equate to a smaller net forcing.
212 Other aerosol changes may have a warming effect. For exam-
213 ple mineral dust levels are generally lower in warm climates,
214 and deserts contracted during the Pliocene (10). Interactions
215 of CH₄ with nitrate and sulphate can also enhance radiative
216 forcing (43). Pliocene aerosol effects therefore require further
217 study.

218 The climate simulations could be benchmarked with
219 Pliocene climate reconstructions. Though no global compila-
220 tions of precipitation change are available for the Pliocene,

individual records can provide informative constraints. The
West African monsoon was probably stronger during the mid-
Pliocene even when compared to the early to mid-Holocene
(44). There was also a general drying trend in East Africa
during the Pliocene (45), which if continued to the present,
implies wetter conditions during the mid-Pliocene. Both of
these features are most faithfully reproduced in HadCM3 and
GISS and the Eoi⁴⁰⁰ IPSL simulation (see SI Appendix, Fig.
S2). In Asia, a reconstructed near-doubling of precipitation in
Southern China (46) is replicated in IPSL (Eoi⁴⁰⁰ simulation)
and by HadCM3 but not the other models. Only HadCM3 and
CCSM4 simulate wetter conditions reconstructed for the early
to mid-Pliocene in Australia (47). One of the regions of largest
inter-model spread in precipitation is tropical South America,
but to our knowledge quantitative precipitation records have
yet to be produced.

HadCM3 has the strongest warming globally and in particu-
lar over most land masses and over the North Atlantic, where
most other models significantly underestimate reconstructed
warming (6). HadCM3 model also shows among the best
agreement with the available temperature reconstructions(10).
This lends support to the stronger methane forcing that is sim-
ulated with the HadCM3 climate drivers, since the enhanced
warming, particularly over land and associated hydrological
cycle changes, promote trace gas emissions. A global biome
reconstruction could also provide some measure to discern
between simulations (48), but this is initially derived from a
simulation with HadCM3, and so is very likely biased towards
the climatic response of this model.

B. Likely non-CO₂ Climatic Response. Our modelling study
probably underestimates the true magnitude of the Pliocene
methane cycle feedback, because the climate and methane cycle
are not coupled. The feedback of methane radiative forcing
via climate to methane emissions is not complete, and all of
the simulated climates underestimate mid- and high-latitude
warming over land considerably (10). Furthermore, our study
has a relatively modest change in wetland area compared with
modelling studies of earlier warm periods (26, 28, 49), and
so the resultant radiative forcing is potentially a conservative
prediction. Any additional warming resulting from the higher
concentrations of trace gases including methane, would further
perturb the sources and atmospheric chemistry. Using the
upper and lower limits for the γ_{fCH_4} , we can approximate
this. The trace gas forcing-induced warming would lead to
an additional methane feedback bringing the total Pliocene
methane radiative forcing to 0.62-1.1 Wm⁻². These total non-
CO₂ values are 33-56% of the CO₂ radiative forcing, with a
central estimate of 0.9 Wm⁻² or 43% of the CO₂ forcing. This
would cause a warming of 0.6-1.0 °C (see table 1).

This is an important additional warming signal given that
PlioMIP phase 1 GCMs forced only with increased CO₂ show
a response of 2.7 ± 0.8 K (16). To better understand the
regional impacts of this additional radiative forcing we analyse
mid-Pliocene simulations from HadCM3 with prescribed levels
of atmospheric CO₂. The CO₂ radiative forcing differences
relative to the default Eoi⁴⁰⁰ are approximately 0.66 Wm⁻²
for the increase by 50 ppmv and 1.1 Wm⁻² for the increase
to 490 ppmv. These encompass the range of non-CO₂ GHG
radiative forcing we calculated (0.62-1.1 Wm²). The effective
radiative forcing (or the temperature change per unit increment
of radiative forcing) is actually higher for CH₄ and N₂O than

for CO₂, and it is lower for O₃ (51). For simplicity here we assume that they are all equal.

The Pliocene HadCM3 simulations with differing CO₂ concentrations show significant polar amplification, especially in the Northern hemisphere and around the Atlantic see figure 3. The Eoi⁴⁵⁰ and Eoi⁴⁹⁰ simulations show relatively muted warming signal in the circum-Atlantic, because of a reduction in heat transport in the Atlantic (50). The upper-end of our estimated radiative forcing, represented by the Eoi⁴⁹⁰ simulation, is shown in figure 3b. This estimated non-CO₂ GHG radiative forcing (figure 3c) causes high-latitude temperatures to increase by around 1-2.5°C over land and by 1-2°C over the ocean surface (figure 3 and see SI Appendix, Fig. S3). This does not eliminate the large mismatches found over high latitude Asia (figure 3c,d) and in the North Atlantic (see SI Appendix, Fig. S3), but it improves the comparison with the temperature reconstructions by (10) as shown in figure 3d. The distribution of errors is shifted from having a significant probability over the range -5 to -1°C to being approximately centred on 0°C. For HadCM3, both the smaller and larger increases in radiative forcing improve the model-data agreement, except for sites with very high temperatures at high-latitudes. The very high temperatures in high-latitude regions would very likely further enhance trace gas emissions, especially CH₄ from wetlands, and so reinforce the positive radiative forcing.

Reasons for the enduring high-latitude discrepancies might include seasonal bias in reconstructions over land or ocean (52), and long-term trends in seawater chemistry (53). If the reconstructions capture peak warmth during orbital cycles, this may not be adequately captured by climate model simulations with pre-industrial orbital configuration (54), and global assemblages of reconstructions may capture different phases of Earth's orbit in different locations (10), further complicating comparisons with simulations. Terrestrial reconstructions are also potentially influenced by the dependence of plant water-use efficiency on atmospheric CO₂, and changes in seasonality and the frequency of extreme events (55). However, a general underestimation in polar amplification of past warm states, could signify systematic problems with climate model parameterisations of clouds (56, 57) and/or aerosol-cloud interactions (58).

These model results allow an estimate of $S_{LI,GHG}$, the temperature response per unit of radiative forcing due to ice-sheets and sea-level (LI) and due to greenhouse gases (GHG) (K/Wm⁻²), where S_{LI,CO_2} was possible until now (4). Several studies have considered the Earth System Sensitivity, the long-term temperature response to changes in radiative forcing, incorporating vegetation and ice-sheet responses (5). Our central estimate of 43% non-CO₂ greenhouse gas radiative forcing would reduce values estimated from Pliocene temperature reconstructions from around 9°C (59) to 6.5°C. This is still much larger than predicted based on "fast" feedbacks in the climate system, and is therefore potentially consistent with irreversible long-term planetary warming, should we fail to limit warming this century to 1.5°C (8).

4. Conclusions

The mid-Pliocene is a critically important past time period to understand because levels of atmospheric CO₂ were very likely as high as today's anthropogenically perturbed levels, at around 400 ppmv. The Pliocene therefore offers unique

insight into a warmer Earth system at equilibrium (5, 6). CH₄ is the second most important anthropogenic greenhouse gas today, but beyond the ice-core era to 800 ka BP, it has been largely ignored. Whereas for CO₂, proxies have been developed to reconstruct its evolution for deep times, no such proxy exists for CH₄. We used vegetation model simulations and an offline CH₄ budget model to produce a comprehensive set of simulations quantifying the likely CH₄ emissions, lifetime and concentration during this time period, investigating changes of methane sources and sinks but excluding abrupt releases derived from clathrates or permafrost degradation. We show that there is a direct net positive radiative forcing of 0.22 Wm⁻² (range 0.1-0.45), which when combined with estimates of radiative forcing from N₂O and O₃ leads to an additional radiative forcing that is between 36-56% of that caused by a CO₂ concentration of 400 pmv. This would likely cause an additional global mean warming of approximately 0.6-1.0 °C at the global scale. Terrestrial trace gas radiative forcing is therefore critically important for understanding the reconstructed warmth of the Pliocene. We suggest that the first-order estimates of these additional forcing agents could help to reconcile model and proxy-based estimates of Pliocene warmth and that failing to include such forcings will lead to substantial biases in simulations of past climates. Their omission also has consequences when trying to estimate the "fast" or "Charney" climate sensitivity from paleo-data (60). Such methods attempt to remove the slower "Earth System" forcings such as changes in ice sheets and assume the residual changes are due to the fast response to CO₂. However, these estimates have not normally included non-CO₂ trace gases and are therefore potentially overestimating the CO₂ sensitivity.

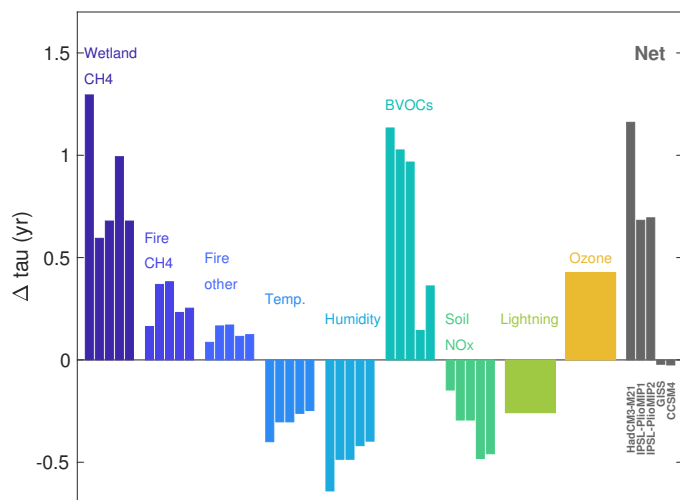


Fig. 1. Simulated mean change in lifetime of CH₄ with respect to OH for the Pliocene minus the pre-industrial, net values and individual terms are shown for the five different sets of climate drivers (HadCM3-M21-Eoi⁴⁰⁰, IPSL-CM5A-PlioMIP1, IPSL-CM5A-Eoi⁴⁰⁰, GISS-E2-R-PlioMIP1, CCSM4-PlioMIP1).

373 **Figures.**

DRAFT

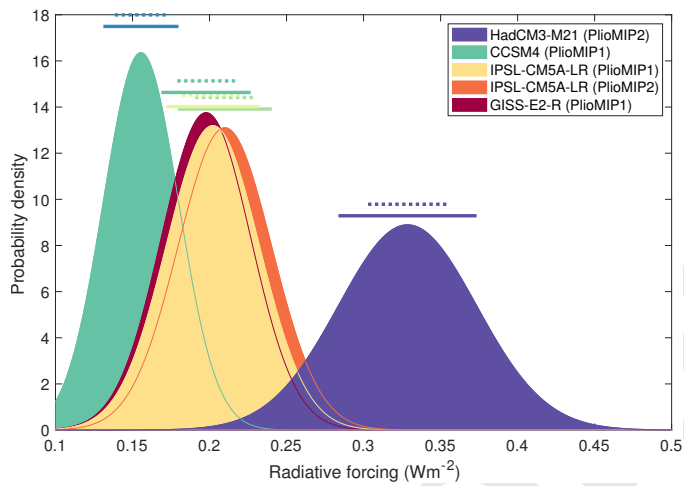


Fig. 2. Estimated radiative forcing expressed as a probability density function. The uncertainty stems from (i) assumed $\pm 20\%$ uncertainties in lightning NO_x and tropospheric O_3 (ii) uncertainty in the parameters used to estimate OH lifetime of CH_4 (37), and (iii) uncertainty in the total radiative forcing due to CH_4 (37, 38). The $\pm 1 \sigma$ uncertainty is shown above each curve. Dashed lines represent first two factors and solid bars underneath include all three sources of uncertainty.

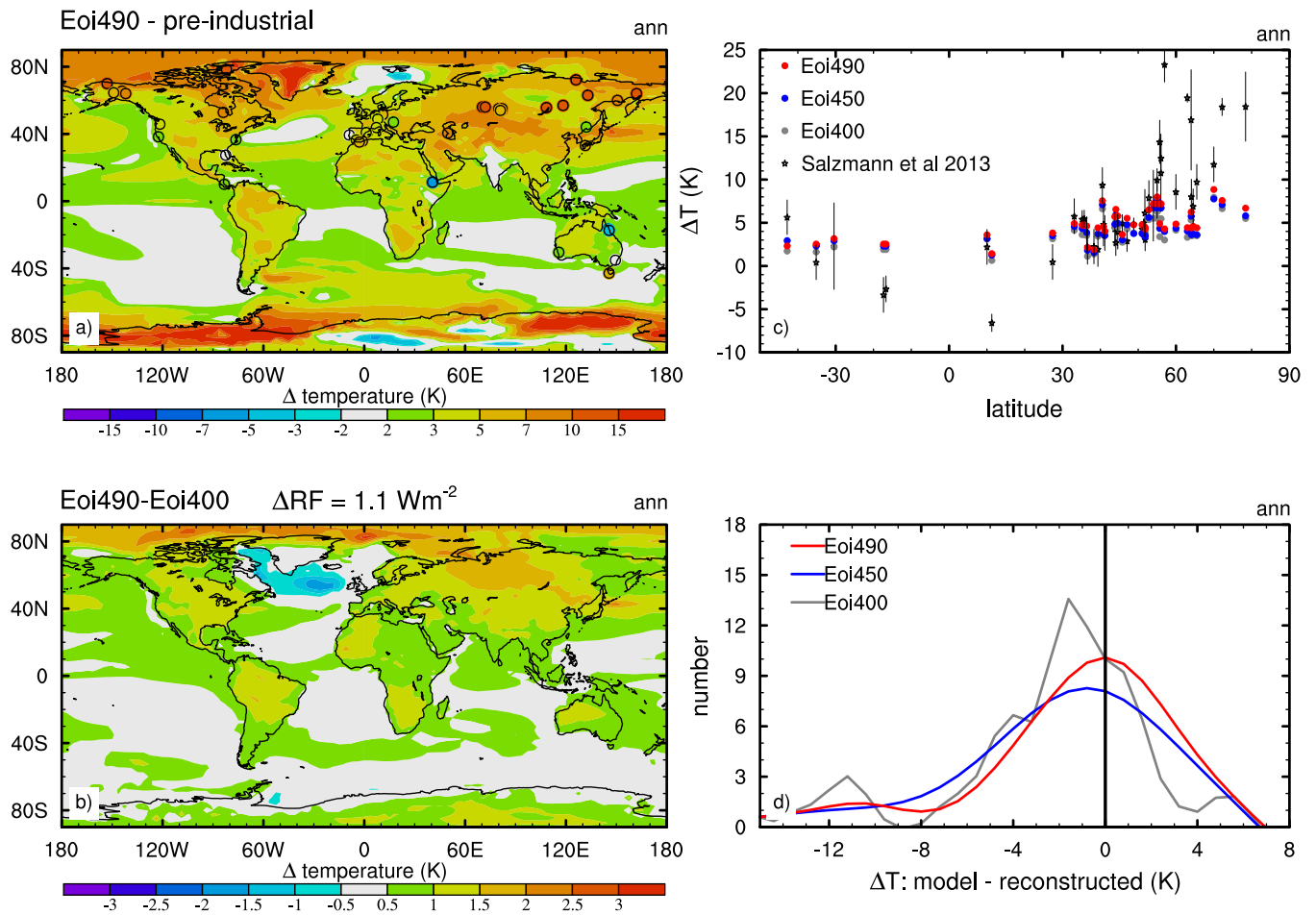


Fig. 3. Simulations with HadCM3-M21 and reconstructions of Pliocene near-surface air temperature change (ΔT) relative to the pre-industrial (K). (a) Simulated (50) and reconstructed (10) ΔT for Eoi⁴⁹⁰ minus pre-industrial, (b) simulated ΔT for Eoi⁴⁹⁰ - Eoi⁴⁰⁰, (c) latitudinal comparison of the reconstructed and simulated temperature anomalies, (d) histogram of model minus reconstruction temperature anomalies.

Table 1. Pliocene radiative forcing, CH₄ cycle sensitivity and predicted non-CO₂-forced warming from this study and past work.

	Mean	Range	Reference
Radiative forcing (Wm⁻²)			
CO ₂	2.0	-	Haywood et al. 2013(17)
CH ₄	0.22	0.10-0.43	This study
N ₂ O	0.33	0.32-0.36	This study
O ₃	0.29	0.28-0.36	Unger & Yue, 2014(20)
Total GHG	2.80	2.67-3.02	This study
Total non-CO ₂	0.80	0.67-1.02	This study
with self-feedback	0.86	0.62-1.12	This study
% of CO ₂	43 %	36-56 %	This study
CH₄ cycle sensitivity to temperature (mWm⁻²K⁻¹)			
Pliocene (3.3-3.0 Ma BP)	100	89-114	This study
Early Eocene (55 Ma BP)	109	97-120	Beerling et al. 2011(28)
Cretaceous (90 Ma BP)	89	-	Beerling et al. 2011(28)
LGM (21 ka BP)	68	57-85	Loulergue et al. 2008; Annan & Hargreaves, 2013 (22, 42)
Global mean temperature change (°C)			
Warming (non-CO ₂)	0.7	0.6-0.9	This study
with self-feedback	0.7	0.6-1.0	This study

375 **Materials and Methods**

376

A. Climate simulations. We use climate simulations from four GCMs: HadCM3-M21, IPSL-CM5A-LR, CCSM4 and GISS-E2-R. These GCMs are compared briefly in SI Appendix, Table S2. They span a reasonable range of changes for Pliocene and incorporate either PlioMIP phase 1 experiment 2 (34, 61) or PlioMIP phase 2 boundary conditions for the Pliocene (17). In all Pliocene simulations, the CO₂ mixing ratio is increased from 280 ppmv in the pre-industrial to 400 (PlioMIP 2) or 405 ppmv (PlioMIP1). The remaining Pliocene boundary conditions are based on geological evidence for orography, land-ice, vegetation and soils, or are left unchanged at pre-industrial settings. For land-ice, the volume of the Greenland ice-sheet is reduced and the West Antarctic ice-sheet is removed. Eustatic sea-level is 25 m above modern. The global vegetation reconstruction prescribes a northwards extension of forests causing a reduction in the area of tundra, whilst deserts are partly replaced by savannah and forest, particularly in the Sahel (10). In PlioMIP phase 1 simulations orography increases over the Rockies and East Antarctica, but these are changes are smaller in PlioMIP phase 2 for which both the Canadian Archipelago and Bering Strait are closed. The remaining model boundary conditions, including orbital configuration, solar constant, mixing ratios of CH₄, N₂O and O₃ and aerosols are as used in the relevant pre-industrial setup.

In PlioMIP1 phase 1, the boundary conditions are referred to as experiment 2 for coupled atmosphere-ocean simulations (34, 61). In PlioMIP phase 2 the nomenclature used is Ex^c, where x can include 'o' and/or 'i' to signify whether or not the orography and land-ice respectively are based on Pliocene geological reconstructions, and 'c' is the prescribed Pliocene CO₂ mixing ratio (17). Since the default PlioMIP phase 2 CO₂ mixing ratio is 400 ppmv, this simulation is labelled Eoi⁴⁰⁰. We also make use of simulations with HadCM3-M21 in which the CO₂ mixing ratio is set to 450 or 490 ppmv, and these are labelled Eoi⁴⁵⁰ and Eoi⁴⁹⁰, respectively. The global mean radiative forcing difference relative to the standard Eoi⁴⁰⁰ simulation is therefore approximately 0.7 and 1.1 Wm⁻², for Eoi⁴⁵⁰ and Eoi⁴⁹⁰, respectively. These increases therefore encompass the upper and lower end of our estimated additional non-CO₂ radiative forcing listed in table 1.

B. Vegetation model simulations. We simulate the land surface with the dynamic stand-based global vegetation model LPJ-GUESS v3 (31, 32). LPJ-GUESS was forced with repeating 30 years of monthly fields from the four GCMs listed above. A 500 year spin up to equilibrium was conducting using repeating the 30-year climate data prior to each 30 year simulation. We expand the land-sea-mask using coastlines from PlioMIP phase 2 (17), including a partially deglaciated Greenland. The soil type over new land points is extrapolated from nearby existing points using the default soil type in LPJ-GUESS. CO₂ was set to 280 and 400 ppmv for pre-industrial and Pliocene simulations, respectively.

C. Trace gas emissions. Wetland area is calculated from the GCM soil moisture using a TOPMODEL approach (62), in which the fractional area of inundation is calculated from the probability density function within each gridcell as derived from global high-resolution topographic data. CH₄ emissions are a function of microbial activity i.e. temperature, available substrate and wetland area (63). Total pre-industrial emissions are scaled to 140 TgCH₄/yr for each model, consistent with the observed methane isotope and concentration measurements (64).

Termite CH₄ emissions are calculated from the LPJ-GUESS simulated plant functional types (PFTs) coverage and observed emission per biome type (30, 65). Isoprene and monoterpene emissions and biomass burning are represented with process-based schemes coupled within LPJ-GUESS (66–68). We estimate soil emissions of nitrogen oxides (NO_x) using a recently developed semi-empirical scheme(69).

441 **D. CH₄ chemical lifetime and radiative forcing.** We calculate the up-
442 take of CH₄ in soils with a process-based model (70) driven with
443 climatologies from the GCMs. For the OH lifetime τ , we inte-
444 grate the Pliocene changes in emissions of all of the above species
445 as well as atmospheric conditions and composition. As a full 3D
446 chemistry-transport simulation is extremely computationally expen-
447 sive, it would limit the evaluation of uncertainty. Hence we employ
448 a parametric model (37) which is calibrated with three coupled
449 climate-chemistry transport models. This model is described in the
450 SI.

451 We combine the CH₄ source estimates with the lifetime calcula-
452 tion in a global-mean budget calculation $B = S \times \tau$, where B is the
453 atmospheric CH₄ burden in Tg, S is the global mean CH₄ source
454 and τ is the lifetime in years (64). The budget equation is combined
455 with the parametric lifetime model and the soil uptake, which is
456 multiplied by the resultant concentration divided by pre-industrial
457 value. This is solved iteratively, to account for the self-feedback of
458 CH₄ on lifetime and soil uptake.

459 The methane radiative forcing is a combination of direct and
460 indirect components which are given in the SI Appendix, Table S4.
461 The total is $0.8 \pm 0.09 \text{ Wm}^{-2}$ per 1000 ppbv increase in atmospheric
462 CH₄.

463 To account for uncertainties, we prescribe a standard deviation
464 of $\pm 20\%$ for lightning NO_x and stratospheric O₃, which are not
465 simulated directly. We include uncertainties inherent in the CH₄
466 lifetime and radiative forcing calculations as described in the SI and
467 and example is shown in SI Appendix, Table S5. The calculations
468 are sampled with 10,000 evaluations of the iterated global CH₄
469 budget formulation.

470 **E. Data availability.** GCM simulation output for the pre-industrial
471 simulations are available from Earth System Grid Federation CMIP5
472 archive. Pliocene simulations can be obtained through the PlioMIP
473 project. Pliocene geographic boundary conditions used in this
474 study are available from PRISM [https://geology.er.usgs.gov/egpsc/
475 prism/4_data.html](https://geology.er.usgs.gov/egpsc/prism/4_data.html). LPJ-GUESS model outputs and all model code
476 developed in this study have been archived on figshare: [dx.doi.
477 org/10.6084/m9.figshare.12302201](https://doi.org/10.6084/m9.figshare.12302201) (piControl simulations), [dx.doi.org/
478 10.6084/m9.figshare.12302216](https://doi.org/10.6084/m9.figshare.12302216) (PlioMIP1 simulations), [dx.doi.org/10.
479 6084/m9.figshare.12302228](https://doi.org/10.6084/m9.figshare.12302228) (PlioMIP2 simulations) and [dx.doi.org/10.
480 6084/m9.figshare.12344027](https://doi.org/10.6084/m9.figshare.12344027) (emissions and lifetime code). The source
481 code for LPJ-GUESS v4.0 can be obtained on request through
482 Lund University (web.nateko.lu.se/lpj-guess). [HadCM3-M21 Eoi⁴⁹⁰
483 climate fields are archived on figshare: dx.doi.org/10.6084/m9.figshare.
484 12630356](https://doi.org/10.6084/m9.figshare.12630356).

485 **ACKNOWLEDGMENTS.** POH is supported by a University of
486 Birmingham Fellowship. GR is supported by the French project
487 LEFE "ComPreNdrE" (A2016-992936), French State Program In-
488 vestissements d'Avenir (managed by ANR), ANR HADOC project,
489 grant ANR-17-CE31-0010 of the French National Research Agency.
490 TAMP acknowledges support from the European Research Council
491 under the European Union Horizon 2020 programme (Grant 758873,
492 TreeMort).

493 This work was carried out using the computational facilities
494 of the Birmingham Environment for Academic Research - [http:
495 //www.bear.bham.ac.uk](http://www.bear.bham.ac.uk). We thank Linda Sohl and Mark Chandler
496 from NASA GISS for providing model outputs and Nan Rosenbloom
497 (NCAR) who performed the original CCSM4 simulations. We
498 thank Sophie Szopa for informative discussions on these topics.
499 This is paper number <x> of the Birmingham Institute of Forest
500 Research.

501 **F. References.**

502 1. Seki O, Foster G, Schmidt D, et al. (2010) Alkenone and boron-based Pliocene pCO₂ records. *Earth Planet Sci Letts* 292:201–211.

503 2. Bartoli G, Honisch B, Zeebe R (2011) Atmospheric CO₂ decline during the Pliocene intensification of Northern Hemisphere glaciations. *Paleoceanography* 26:PA4213.

504 3. Badger M, Schmidt D, Mackensen A, Pancost R (2013) High resolution alkenone palaeo-barometry indicates relatively stable pCO₂ during the Pliocene (3.3 to 2.8 Ma). *Phil T.R. Soc. A* 371(20130094):371.

505 4. Martínez-Boti M, et al. (2015) Plio-Pleistocene climate sensitivity evaluated using high-resolution CO₂ records. *Nature* 518:49–54.

506 5. Lunt D, et al. (2010) Earth system sensitivity inferred from Pliocene modelling and data. *Nature Geosci* 3:60–64.

507 6. Haywood A, Dowsett H, Dolan A (2016) Integrating geological archives and climate models for the mid-Pliocene warm period. *Nature Comms* 7:10646.

508 7. Burke K, Williams J, Chandler M, Haywood A, et al. (2018) Pliocene and Eocene provide best analogs for near-future climates. *PNAS* 115(52):13288–13293.

509 8. Steffen W, Rockstrom J, Richardson K, et al. (2018) Trajectories of the Earth System in the Anthropocene. *PNAS* 115(33):8252–8259.

510 9. Tan N, et al. (2018) Modeling Greenland ice sheet evolution during the Plio-Pleistocene transition: new constraints for pCO₂ pathway. *Nature Comms* 9:4755.

511 10. Salzmann U, Dolan A, Haywood A, et al. (2013) Challenges in quantifying Pliocene terrestrial warming revealed by data-model discord. *Nature Climate Change* 3:969–974.

512 11. Dowsett H, et al. (2013) Sea surface temperature of the mid-Piacenzian ocean: a datamodel comparison. *Scientific Reports* 3.

513 12. Foley K, Dowsett H (2019) Community sourced mid-Piacenzian sea surface temperature (SST) data. *U.S. Geological Survey data release*, doi: 10.5066/9P9Y3D7V.

514 13. Miller K, et al. (2012) High tide of the warm Pliocene: implications of global sea level for Antarctic deglaciation. *Geology* 40:407–410.

515 14. Dutton A, Carlson A, Lnog A, Milne G, et al. (2015) Sea-level rise due to polar ice-sheet mass loss during past warm periods. *Science* 349(6244):aaa4019–1.

516 15. Dumitru O, Austermann J, Polyak V, Fornos J, et al. (2019) Constraints on global mean sea level during Pliocene warmth. *Nature* 574:233–236.

517 16. Haywood A, et al. (2013) Large-scale features of Pliocene climate: results from the Pliocene Model Intercomparison Project. *Clim Past* 9:191–209.

518 17. Haywood A, Dowsett H, Dolan A, Rowley D, et al. (2016) The Pliocene Model Intercomparison Project (PlioMIP) Phase 2: scientific objectives and experimental design. *Clim Past* 12:663–675.

519 18. Robinson M, et al. (2011) Bathymetric controls on Pliocene North Atlantic and Arctic sea surface temperature and deepwater production. *Palaeogeog, Palaeoclim, Palaeoecol* 309(1–2):92–97.

520 19. Otto-Bliesner B, Braconnot P, Harrison S, Lunt D, et al. (2017) Two Interglacials: Scientific Objectives and Experimental Designs for CIMP6 and PMP4 Holocene and Last Interglacial Simulations. *Geosci Model Dev* p. .

521 20. Unger N, Yue X (2014) Strong chemistry-climate feedbacks in the Pliocene. *Geophys Res Lett* 41(527–533).

522 21. Myhre G, et al. (2013) Anthropogenic and Natural Radiative Forcing in *Climate Change 2013: The Physical Science Basis: Contribution of Working Group I to the Fifth Assessment Report of the Intergovernmental Panel on Climate Change*, eds. Stocker T, et al. (C.U.P., Cambridge, U.K. and New York, U.S.A.), pp. 659–740.

523 22. Loulergue L, et al. (2008) Orbital and millennial-scale features of atmospheric CH₄ over the past 800,000 years. *Nature* 453(7243):383–386.

524 23. Rhodes R, et al. (2015) Enhanced tropical methane production in response to iceberg discharge in the North Atlantic. *Science* 348:1016–1019.

525 24. Schilt A, et al. (2010) Glacial-interglacial and millennial scale variations in the atmospheric nitrous oxide concentration during the last 800,000 years. *Quaternary Sci. Rev.* 29:182–192.

526 25. Valdes P, Beerling D, Johnson C (2005) The ice age methane budget. *Geophys. Res. Lett.* 32(L02704).

527 26. Beerling D, Berner R, Mackenzie F, Harfoot M, Pyle J (2009) Methane and the CH₄-related greenhouse effect over the past 400 millions years. *American Journal of Science* 309:97–113.

528 27. Holmes C (2018) Methane Feedback on Atmospheric Chemistry: Methods, Models, and Mechanisms. *J Advances in Modeling Earth Systems* 10:1087–1099.

529 28. Beerling D, Fox A, Stevenson D, Valdes P (2011) Enhanced chemistry-climate feedbacks in past greenhouse worlds. *Proc Natl Acad Sci USA* 108:9880–9775.

530 29. Singarayer J, Valdes P, Friedlingstein P, Nelson S, Beerling D (2011) Late Holocene methane rise caused by orbitally controlled increase in tropical sources. *Nature* 470:82–85.

531 30. Hopcroft P, Valdes P, O'Connor F, Kaplan J, Beerling D (2017) Understanding the glacial methane cycle. *Nature Communications* 8(14383).

532 31. Smith B, Prentice I, Sykes M (2001) Representation of vegetation dynamics in the modelling of terrestrial ecosystems: comparing two contrasting approaches within European climate space. *Global Ecology and Biogeog* 10:621–637.

533 32. Smith B, et al. (2014) Implications of incorporating N cycling and N limitations on primary production in an individual-based dynamic vegetation model. *Biogeosciences* 11:2027–2054.

534 33. Ruppel C, Kessler J (2017) The interaction of climate change and methane hydrates. *Rev Geophysics* 55:126–168.

535 34. Haywood A, Dowsett H, Otto-Bliesner B, et al. (2011) Pliocene Model Intercomparison Project (PlioMIP): experimental design and boundary conditions (Experiment 2). *Geosci Model Dev* 4:571–577.

536 35. Dowsett H, Robinson M, Haywood A, et al. (2010) The PRISM3D paleoenvironmental reconstruction. *Stratigraphy* 7:123–139.

537 36. Dowsett H, Dolan A, Rowley D, et al. (2016) The PRISM4 (mid-Piacenzian) paleoenvironmental reconstruction. *Clim Past* 12:1519–1538.

538 37. Holmes C, Prather M, Sovde O, Myhre G (2013) Future methane, hydroxyl, and their uncertainties: key climate and emission parameters for future predictions. *Atmos Chem Phys* 13:285–302.

539 38. Etminan M, Myhre G, Highwood E, Shine K (2017) Radiative forcing of carbon dioxide, methane, and nitrous oxide: A significant revision of the methane radiative forcing. *Geophys Res Lett* 43:12614–12623.

540 39. Voulgarakis A, et al. (2013) Analysis of present day and future OH and methane lifetime in the ACCMIP simulations. *Atmos Chem Phys* 13:2563–2587.

541 40. Hansen J, Sato M, Kharecha P, et al. (2007) Climate change and trace gases. *Phil Trans R Soc A* 365(1856):1925–1954.

542 41. Ringeval B, Friedlingstein P, Koven C, et al. (2011) Climate-CH₄ feedback from wetlands and its interaction with the climate-CO₂ feedback. *Biogeosciences* 8:2137–2157.

543 42. Annan J, Hargreaves J (2013) A new global reconstruction of temperature changes at the Last Glacial Maximum. *Climate of the Past* 9:367–376.

544 43. Shindell D, et al. (2009) Improved attribution of climate forcing to emissions. *Science* 326:716–718.

545 44. Kuechler R, Dupont L, Schefuss E (2018) Hybrid insolation forcing of Pliocene monsoon dynamics in West Africa. *Clim Past* 14:73–84.

546 45. Liddy H, Feakins S, Tierney J (2016) Cooling and drying in northeast Africa across the Pliocene. *Earth Planetary Science Letters* 449:430–438.

547 46. Su T, Jacques F, Spicer R, et al. (2013) Post-Pliocene establishment of the present monsoonal climate in SW China: evidence from the late Pliocene Longmen megafloora. *Clim Past* 9:1911–19020.

548 47. Christensen B, Renema W, Henderiks J, et al. (2017) Cooling and drying in northeast Africa across the Pliocene. *Geophys Res Lett* 44:6914–6925.

549 48. Salzmann U, Haywood A, Lunt D, Valdes P, Hill D (2008) A new global biome reconstruction and data-model comparison for the Middle Pliocene. *Global Ecol Biogeogr* 17:432–447.

550 49. Wilton D, Badger M, Kantzas E, et al. (2019) A predictive algorithm for wetlands in deep time paleoclimate models. *Geosci Model Dev* 12:1351–1364.

551 50. Hunter S, Haywood A, Dolan A, Tindall J (2019) The HadCM3 contribution to PlioMIP Phase 2. *Clim Past* 15:1691–1713.

552 51. Hansen J (2005) Efficacy of climate forcings. *J Geophys Res* 110:D18104.

553 52. Tierney J, Tingley M (2016) BAYSPLINE: A New Calibration for the Alkenone Paleothermometer. *Paleoceanography and Paleoclimatology* 33:281–301.

554 53. Evans D, Brierley C, Raymo M, et al. (2016) Planktic foraminifera shell chemistry response to seawater chemistry: Pliocene–Pleistocene seawater Mg/Ca, temperature and sea level change. *Earth Planet Sci Letts* 438:139–148.

555 54. Prescott C, Haywood A, Dolan A, et al. (2014) Assessing orbitally-forced interglacial climate variability during the mid-Pliocene Warm Period. *Earth Planet Sci Letts* 400:261–271.

556 55. Harrison S, Bartlein P, Prentice I (2016) What have we learnt from palaeoclimate simulations? *J Quat Sci* 31(4):364–385.

557 56. Sagoo N, Valdes P, Flecker R, Gregoire L (2013) The Early Eocene equable climate problem: can perturbations of climate model parameters identify possible solutions? *Phil Trans Roy Soc A* 371(2001):20130123.

558 57. Zhu J, Poulsen C, Tierney J (2019) Simulation of Eocene extreme warmth and high climate sensitivity through cloud feedbacks. *Science Advances* 5(9):eaax1874.

559 58. Kiehl J, Shields C (2013) Sensitivity of the Pliocene–Pleistocene thermal maximum climate to cloud properties. *Phil Trans R Soc A* 371.

560 59. Pagani M, Liu Z, LaRiviere J, Ravel A (2010) High Earth-system climate sensitivity determined from Pliocene carbon dioxide concentrations. *Nature Geoscience* 3:27–30.

561 60. PALEOSENS Project Members (2012) Making sense of palaeoclimate sensitivity. *Nature* 491:683–691.

562 61. Haywood A, Dowsett H, Otto-Bliesner B, et al. (2010) Pliocene Model Intercomparison Project (PlioMIP): experimental design and boundary conditions (Experiment 1). *Geosci Model Dev* 3:227–242.

563 62. Zhang Z, Zimmermann N, Kaplan J, Poulter B (2016) Modeling spatiotemporal dynamics of global wetlands: comprehensive evaluation of a new sub-grid TOPMODEL parameterization and uncertainties. *Biogeosciences* 13:1387–1408.

564 63. Gedney N, Cox P, Huntingford C (2004) Climate feedback from wetland methane emissions. *Geophys. Res. Lett.* 31(L20503).

565 64. Hopcroft P, Valdes P, Kaplan J (2018) Bayesian analysis of the glacial-interglacial methane increase constrained by stable isotopes and Earth System modelling. *Geophys Res Lett* 45:3653–3663.

566 65. Sanderson M (1996) Biomass of termites and their emission of methane and carbon dioxide: A global database. *Glob Biogeochem Cy* 10(4):543–557.

567 66. Arneth A, et al. (2007) CO₂ inhibition of global terrestrial isoprene emissions: Potential implications for atmospheric chemistry. *Geophys. Res. Lett.* 34(L18813).

568 67. Schurgers G, Arneth A, Holzinger R, Goldstein A (2008) Process-based modelling of biogenic monoterpene emissions: Sensitivity to temperature and light. *Atmos Chem Phys* 2:43–57.

569 68. Thonicke K, Venevsky S, Stith S, Cramer W (2001) The role of fire disturbance for global vegetation dynamics: coupling fire into a Dynamic Global Vegetation Model. *Global Ecology and Biogeog* 10:661–677.

570 69. Hudman R, et al. (2012) Steps towards a mechanistic model of global soil nitric oxide emissions: implementation and space based-constraints. *Atmos Chem Phys* 12:7779–7795.

571 70. Murguía-Flores F, Arndt S, Ganesan A, et al. (2018) Soil Methanotrophy Model (MeMo v1.0): a process-based model to quantify global uptake of atmospheric methane by soil. *Geosci Model Dev* 11:2009–2032.